European Journal of Mechanics / B Fluids 75 (2019) 219–227

Contents lists available at ScienceDirect

European Journal of Mechanics / B Fluids

journal homepage: www.elsevier.com/locate/ejmflu

Experimental study on the scour due to a water jet subjected to lateral confinement

Román G. Martino [a,*], Francisco García Ciani [b], Agnes Paterson [c], Marcelo F. Piva [b]

[a] CONICET and Grupo de Medios Porosos, Facultad de Ingeniería, Universidad de Buenos Aires, Paseo Colón 850 (1063), Buenos Aires, Argentina
[b] Grupo de Medios Porosos, Facultad de Ingeniería, Universidad de Buenos Aires, Paseo Colón 850 (1063), Buenos Aires, Argentina
[c] Departamento de Hidráulica, Facultad de Ingeniería, Universidad de Buenos Aires, Las Heras 2214(1127), Buenos Aires, Argentina

ARTICLE INFO

Article history:
Received 3 June 2018
Received in revised form 8 October 2018
Accepted 14 October 2018
Available online 19 October 2018

Keywords:
Local erosion process
Inner–outer crater
Laterally constrained water jet

ABSTRACT

The effect of lateral confinement due to very close side walls, on erosion caused by a water jet issuing from a rectangular sluice aperture, has been studied experimentally in a narrow laboratory flume. Velocimetry (PIV) in presence of a smooth, no erodible bottom, revealed self-similar velocity profiles with the structure of a wall jet, but upward-shifted with respect to the classical two-dimensional profile. The classical definition of the Shields number was modified, to include the influence of the relative roughness and the inlet aspect ratio. This last coefficient was also relevant in the definition of a suitable length scale to account for the effect of the lateral confinement. Scour patterns in the narrow flume have also shown differences with respect to erosion by two-dimensional wall jets: the downstream mound undergoes a morphological transition, from triangular to trapezoidal, at the early stage of the scour development, and grains move downhill driven by gravity inside the granular wedge, in a regime of steady recirculation (SR). Above this regime, a digging–refilling (DR) cycle, with periods of the order of seconds, triggers at a well-defined Shields number.

1. Introduction

Sediment transport driven by water jets spreading along narrow gaps is present in nature and in practical applications. It plays a key role in processes involving solid particles dragged through fractures [1], filtration devices, in the emergence and progress of underground channelizations, in wastewater flows discharged in deep and narrow precast drains, and in the motion of solids conveyed in pipelines [2,3]. Techniques for crude oil extraction require detailed studies about slot jet features [4], and laboratory research of proppant transport in slot flow model has shown that, near the fracture entrance, significant sand transport is provided by stimulated turbulence [5,6], which can be produced by pumping fluid through holes in a plate across the slot inlet. Shallow, turbulent water jets are used as a framework to study hydrodynamics and depositional patterns at the mouths of distributary channels [7] because the turbulence characteristics of these narrow, planar bounded jets differ from those of unbounded ones. Contractions of a water stream by debris accumulation could lead to the local scour of the granular bed, due to the local convective acceleration of the flow which increases bed shear stress and the lift action from turbulent bursts [8]. Numerical results in configurations where a narrow receiving channel is located downstream of a sluice gate have shown that increasing lateral confinement modifies the hydrodynamics of the wall jet, increasing the propagation further in the streamwise direction, and reducing the bed shear stress because of the side-walls friction [9]. This last result has also been reported in steady, uniform flow in smooth narrow channels with the rectangular cross-section, and was attributed to the increasing influence of the secondary currents and the fluid shear stresses (reflecting the effect of eddy viscosity in turbulent flows) as the ratio between channel width to flow depth decreases [10]. Side walls (two parallel walls confining the jet at the planes of the short sides of the rectangular nozzle) have been used to force the jet to entrain only in the streamwise and lateral directions, enhancing the two-dimensionality of the flow [11,12]. It has been shown that the large-scale flow organization, for turbulent slot jets bounded by very close solid side walls, differs substantially from the slot free jet, due to the development of the shear layers on both sides (affecting the spreading of the developed jet) and secondary longitudinal vortical structures near the nozzle exit [13].

In spite of its relevance, the influence of side walls proximity on the scour of the bed, immediately downstream of the jet inlet, is still poorly understood and documented. Measurements of the scour caused by a jet issuing from a nozzle of constant aperture, $b_0 = 2$, 5 cm, in a channel of 15 m long and four values of width, w: 10, 20, 30 and 40 cm [14], revealed that w significantly affects the scour patterns. The authors also observed that the confining effect tends to become significant with increasing the mean flow velocity

* Corresponding author.
E-mail address: rgmartino@conicet.gov.ar (R.G. Martino).

https://doi.org/10.1016/j.euromechflu.2018.10.009
0997-7546/

at the inlet plane, U_0. They proposed the inlet aspect ratio, $AR = w/b_0$, as the suitable parameter to account for the confinement effect. From the comparison of their results, in the range $4 \leq AR \leq 16$, with results from wide channels, $AR \gg 1$, they observed that some points do not gather along the same curve. They found cycles of digging (when the jet is directed towards the bed) and refilling (with the jet directed towards the free surface and the grains on the mound rolling back and refilling the hole), which depend on U_0 and relative submergence, H/b_0, being H the tailwater depth. As w increased, it took a longer duration for the initial flipping of the jet towards the free surface to occur. Experimental results showed that the erosion threshold of an immersed granular layer, impinged by a vertical liquid jet issuing from a rectangular injector, $AR = 6$, and enclosed in a rectangular tank, is governed by a critical Shields number of inertial nature, $Sh_0 = \rho U_0^2/((\rho_s - \rho)gd_s)$, being $U_0 = Q/(wb_0)$, Q the flowrate, ρ_s and ρ the densities of the sediment and the fluid, respectively, g is the local gravity acceleration, and d_s the median grain size [15]. The results from this model quasi-two-dimensional set-up have shown that Sh_0 increases non-uniformly with the nozzle-sediment distance, l. This non-uniform evolution was linked to the spatial structure of the jet, related to its flow regime described by the Reynolds number at the inlet, $U_0 b_0/\nu$, where $\nu = \mu/\rho$ is kinematic viscosity.

The scarcity of experimental data on the scour process in channels with a very high degree of lateral confinement is in contrast with a large amount of research work devoted to the scour caused by plane ($AR \gg 1$) wall jets [16,17]. For a layer of non-cohesive sediments immediately downstream of a rectangular opening, b_0, the variation of the scour dimensions with the logarithm of time was found to be linear, and the scour process eventually attains an asymptotic stage, after several hours [18]. The maximum eroded depth, Y_∞, made dimensionless with b_0, was found to be mainly dependent on the densimetric Froude number, $F_0 = Sh_0^{1/2}$ [19,20]. It has been claimed that the effect of grain size is not completely absorbed by F_0 [21,22], hence relative roughness, d_s/b_0, should be included in the analysis. Digging and refilling cycles have been also reported for $AR \gg 1$, in experiments lasting hundreds of hours, being associated with jet-flipping (a phenomenon in which the jet suddenly flips from the bed to the water surface, and vice-versa) [19,23].

It is expected that the hydrodynamics of the wall jet in channels with very close side walls, $AR \sim O(1)$, as well as the scour profiles driven by such highly laterally confined jets, will differ from those reported in configurations with $AR \gg 1$. The question arises on whether the dimensionless numbers, used in this latter case, can be modified, in a physically-meaning way, to account for scour with low values of AR. To this end, experiments on the erosion of a loose granular bed, immediately downstream a sluice gate, were carried out in a narrow laboratory flume. Velocimetry (PIV) over a smooth, no erodible bed, was performed to characterize the mean velocity profiles for the laterally constrained wall jet. The temporal evolution of the eroded bed morphology, lasting several hours, was registered from the beginning by means of a sequence of high spatial resolution snapshots.

2. The experimental setup

Experiments were carried out in a narrow channel, $w = 2$ cm wide and 140 cm long, see Fig. 1. Glass side walls ensured full optical access along the channel. Water flow was driven by a centrifugal pump. Flow rate, Q, was measured with a rotameter of accuracy $\pm$ 0.25 l/min. Water temperature was around 20 °C in all runs. A granular column of packed glass beads was used to generate a uniform velocity distribution at the channel inlet.

The water stream was forced to flow beneath a sluice gate, composed of a vertical acrylic bar of square section, with a 45° sharp edge at the end. Five sluice apertures, b_0, were used. Table 1 summarizes the values of the experimental control variables, Q and b_0. The complete sealing between the inner channel walls and the acrylic bar was verified at each run, to avoid undesirable flow leaks. The mean velocity of the jet at the aperture was calculated as $U_0 = Q/(wb_0)$, and the Reynolds number of the jet, based on the hydraulic diameter of the opening, D_h:

Table 1
Summary of experimental configurations.

b_0 [cm]	Q [l/min]	Re_0	θ_0	Marker
0.2	2.5 – 3.0	3790 – 4550	46.9 – 67.5	+
1.0	3.5 to 12.0	3890 to 13330	2.8 to 32.4	□
1.5	4.5 to 17.0	4290 to 16200	1.9 to 27.4	◯
2.0	5.5 to 17.5	4580 to 14580	1.6 to 15.8	△
4.0	12.0 to 17.0	6670 to 9440	1.7 to 3.5	◊

$$Re_0 = \frac{U_0 D_h}{\nu} \tag{1}$$

with $\nu = 0.01$ cm^2/s the kinematic viscosity of water, ranged between $3790 \leq Re_0 \leq 16200$, see Table 1. Thus, experiments were performed under moderate turbulent jets. The hydraulic diameter, defined as:

$$D_h = \frac{4wb_0}{2w + 2b_0} = \frac{2b_0}{1 + \frac{b_0}{w}} \tag{2}$$

is postulated as the suitable length scale for our configurations, since the proximity of the side walls makes its influence not negligible. From Eq. (2), it follows that D_h/b_0 is a monotonically increasing function of $AR = w/b_0$, and $D_h \to 2b_0$ as $AR \to \infty$: in wide channels ($w \gg b_0$), $D_h \approx 2b_0$ which is the characteristic length scale for two-dimensional jets (disregarding the factor 2) [18,24].

A flat granular layer, 10 cm depth and 60 cm in length, composed of monodisperse glass beads of median diameter $d_s = 1.1$ mm, geometrical standard deviation $\sigma_g = 1.1$ and density $\rho_s = 2.65$ g/cm^3, was placed immediately downstream of the jet inlet. As the ratio $w/d_s \approx 20$, a negligible influence of side walls friction on grains motion is expected [25,26]. At the channel outlet, a mesh of variable porosity was used to keep constant the tailwater depth at $H = 13$ cm. Water was allowed to discharge freely into a tank connected to the pump.

The scour process was recorded, from the beginning, with a Nikon D90 camera, controlled via software from a PC. The experimental protocol to start each run was as follows: as Q was increased, via the control valve, the resistance of the mesh at the flume outlet was continuously reduced, to maintain constant the tailwater depth at $H = 13$ cm. Typically, it took only 1 to 2 s to reach steady flow conditions at the inlet. Because each run lasted approximately 9 h, different time spans between successive snapshots were used, accompanying the slowing down of the erosive process with time. In all runs, the profile of the eroded bed remained flat across the channel width, as observed in previous work [14]. Frontal panels of LED light were placed to ensure optimal contrast and definition in the images. In-house software, designed to manage large amounts of images (approximately 1500 per run), allowed to extract the temporal evolution of the coordinates of the bed profile, $(X(t), Y(t))$. Thus, the coordinates of characteristic points, such as the maximum scour depth, Y_∞, and length, X_∞, as well as the characteristic angles of the erosive structures, were easily extracted from each image. The Shields number for the erosive process was defined as:

$$\theta_0 = \left[\frac{d_s}{D_h}\right]^{2\gamma_1} \frac{\rho U_0^2}{(\rho_s - \rho)gd_s} = \left[\left(\frac{d_s}{b_0}\right)\left(\frac{1 + \frac{b_0}{w}}{2}\right)\right]^{2\gamma_1} Sh_0 \tag{3}$$

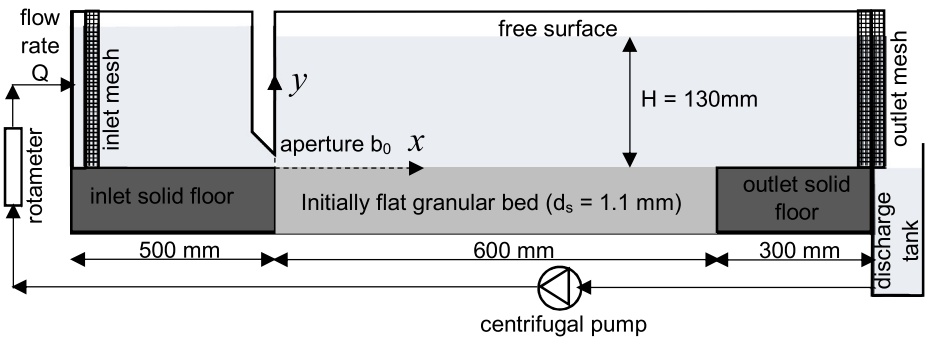

Fig. 1. Sketch of the experimental setup.

with $\gamma_1 = 0.11$ [21]. Thus, θ_0 encapsulates the effects of $Sh_0 = F_0^2$, defined as the ratio between the tractive force of the jet on a grain and its apparent weight, and the relative roughness, d_s/b_0, modulated by a coefficient that takes into account the opening aspect ratio, $AR = w/b_0$. From Eq. (3) it follows that bed friction is assumed to be mainly dependent on d_s/b_0 for the turbulent jet.

3. The base flow at the test section

To characterize the mean flow field induced by the jet in the test section of the narrow flume, time-averaged velocity profiles were measured in the midplane of the channel using PIV for $b_0 = 2$ cm and $U_0 = 33.3$ cm/s. The erodible granular bed was replaced with a dummy, no erodible smooth floor. The Reynolds number, $Re_0 = 6660$, is close to the values used in previous works [27,28] to study a deeply-submerged, plane wall jet of water, running over a smooth bottom. The water was seeded with resin grains, relative density 1.03 and mean size 90 μm, and the vertical midplane was illuminated with a green laser sheet (532 nm Neodimio-Yag of 100 mW). Measurements were performed at five stations along the test section with a CCD monochrome camera, 480 × 640 pixels, at 200 frames per second. The velocity profiles were extracted via the cross-correlation algorithm, using interrogation windows 32 × 32 pixels in size with 50% overlapping. Fig. 2(A) shows typical velocity profiles in the region of fully developed flow, which clearly exhibits the structure of a wall jet. Measurements revealed a predominantly longitudinal flow field, since the vertical velocities, V, were negligible when compared to the longitudinal ones, U.

To test the self-similarity of the velocity distributions, the maximum velocity at any station, U_m, was chosen as velocity scale, and $y_{1/2}$, the distance above the bottom where $U = U_m/2$ and $\partial U/\partial y < 0$, was chosen as the correspondent length scale [29]. Fig. 2(B) show that the dimensionless velocity profiles of the forward flow collapse along a single curve. Thus, self-similarity in outer scales is preserved. For the established-flow zone of a two-dimensional wall jet, it has been shown that the velocity distribution can be described by the following similarity function [30,31]:

$$\frac{U}{U_m} = A_1 \left(\frac{y}{y_{1/2}}\right)^{1/7} \left[1 - erf\left(A_2 \frac{y}{y_{1/2}}\right)\right] \tag{4}$$

with $A_1 = 1.48$ and $A_2 = 0.68$. Eq. (4) is plotted in 2(B) in dashed line. The velocity profiles measured in the narrow flume presents a clear upward shifting when compared with the classical distribution for two-dimensional wall jets. The increase of the inner-boundary layer thickness has been reported in experiments where a plane wall jet flowed in contact with a rough bed [32,33]. The upward-shifting was attributed to the increase in the drag force exerted on the flow by the bottom roughness. In our case, the jet ran over the smooth bottom of a very narrow channel, thus the origin of the upward shift may be mainly attributed to the drag force due to the shear layers, which develop in the close side walls. Induced secondary currents, due to the enhancement in the production of longitudinal vorticity in the lateral boundary layer, could be the responsible for this upward-shifting of the velocity profiles.

Having found self-similar profiles for the forward flow, it is necessary to analyse the variation of U_m and $y_{1/2}$ with the longitudinal distance from the opening, x. Fig. 3(A) shows the decay of U_m/U_0 with x/b_0. It is also drawn, in dashed line, the equation for the decay rate of deeply submerged, two-dimensional turbulent wall jets [27,29]:

$$\frac{U_m}{U_0} = \frac{3.50}{\sqrt{\frac{x}{b_0}}} \tag{5}$$

It is observed that the values of U_m are slightly lower than those expected for two-dimensional wall jet with the same U_0. Besides, velocity decays at a slightly lower rate, $U_m/U_0 \approx 2(x/b_0)^{-1/3}$ ($R^2 = 0.970$), instead of the classical 1/2 power-law. This result is consistent with previous works dealing with planar jets of air, bounded by close side walls [34], where exponents lower than 1/2 were measured for low values of AR. Fig. 3(B) shows the dimensionless growth of the length scale of the jet (half-width). By assuming a linear relationship, the rate of spread is $A = dy_{1/2}/dx \approx 0.081$ ($R^2 = 0.990$), just slightly larger (but still within the experimental uncertainty) than that measured for two-dimensional wall jets, of about 0.077 ± 0.02 [27–29]. Although this topic deserves further research, results suggest a weakening of the jet due to the momentum losses by friction with the side walls. In the next section, it will be shown that associated with this flow field, a characteristic regime of local scour takes place in the narrow flume.

4. Local scour in the narrow flume

4.1. Temporal evolution of the erosive process

Fig. 4 shows a sequence of snapshots taken from a run with $Q = 6.5$ l/min and $b_0 = 1.0$ cm. Each image is labelled with a timestamp. At the early stages of the process, $0 \leq t \leq 12$ s, the jet is tangential to the bed, and the sediment moves as bedload driven by shear stresses in the inner boundary layer. Some grains were observed to move in saltation in runs with large θ_0. Due to the intense and aggressive erosive process, the scour hole quickly develops and grows. The extracted grains settle, after short flights, downstream at the lee side of a triangular mound.

Above $t = t_c \approx 12 - 14$ s, the mound undergoes a morphological transition from triangular to trapezoidal. This rearrangement indicates that the triangular structure is unstable with respect to the competition between the eroding jet and the stabilizing action of gravity. This transition is attributed to the weakness of the jet: when the resistance of the granular mound attains a critical value, the jet cannot support the pile and the system relaxes through

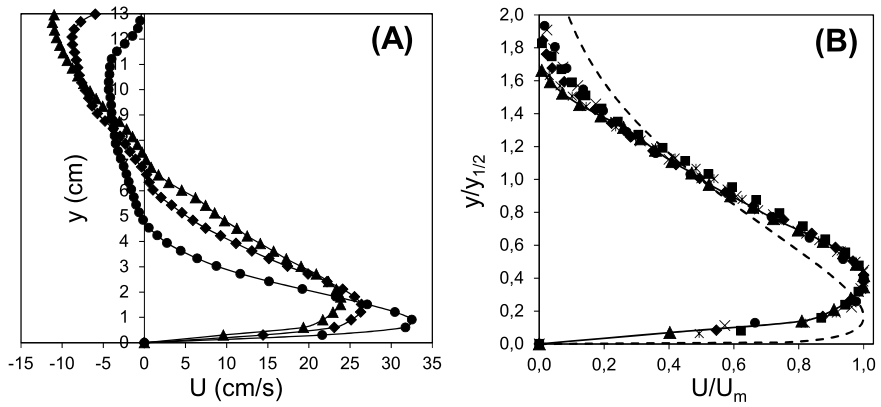

Fig. 2. Self-similarity of streamwise time-averaged velocity profiles in outer scales: (*A*) profiles at different stations, x, in the test section, and (*B*) profiles made dimensionless with U_m and $y_{1/2}$. Markers for stations x are: •17.8 cm, × 22.8 cm, ♦ 30.8 cm, ■35.8 cm, ▲ 41.4 cm and ∗ 48.6 cm. The velocity distribution for a plane wall jet, Eq. (4), is plotted in dashed line.

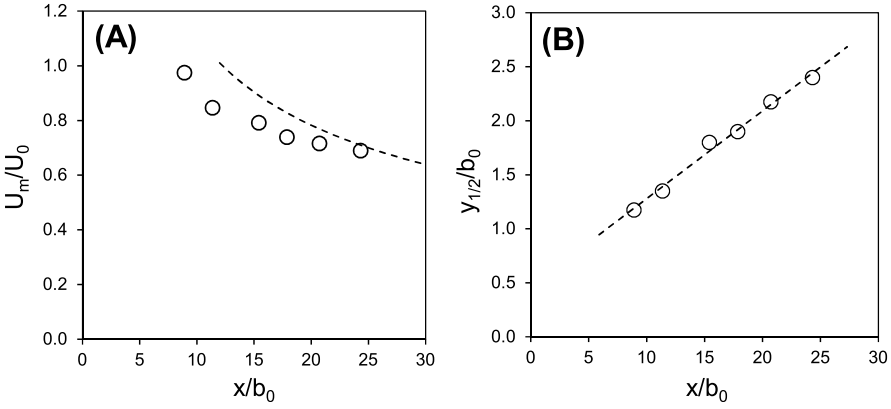

Fig. 3. Variation with x/b_0 for: (*A*) dimensionless maximum velocity, U_m/U_0, and (*B*) velocity half-width, $y_{1/2}/b_0$.

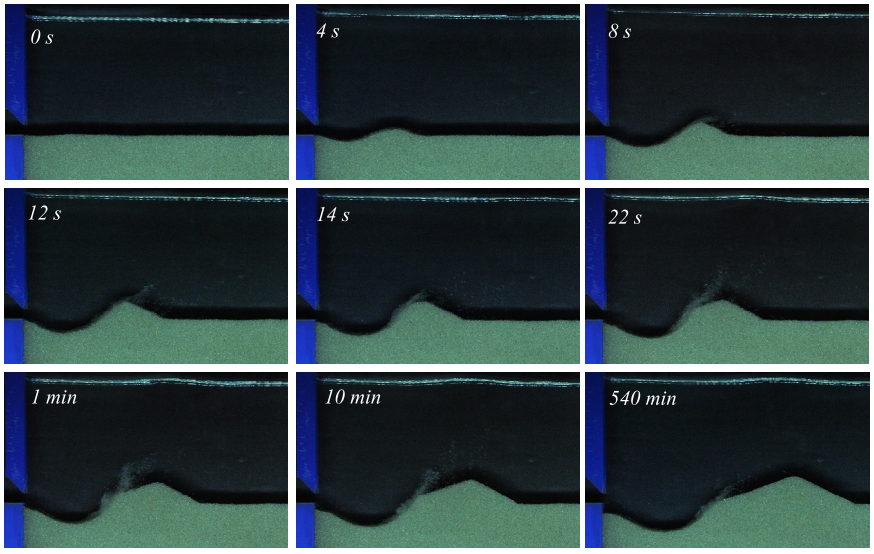

Fig. 4. Temporal evolution of the scour process in a run lasting 9 h, with $Q = 6.5$ l/min and $b_0 = 1.0$ cm.

gravity-driven grains sliding. Such erosive patterns, with inner and outer craters, have also been observed in experiments studying the granular bed impinged by vertical jets [35,36]. Accompanying the morphological transition, the jet undergoes a pronounced deflection towards the free surface. Thus, more and more grains extracted from the hole cease to feed the right-hand side of the mound, but they settle on its left side (plateau of accumulation).

Fig. 5(A) shows that t_c decreases with Q and increases with b_0, suggesting a dependence with Q/b_0. Indeed, when t_c is plotted against θ_0, the points gather along a single decreasing curve, see Fig. 5(B). From this curve, three regions can be identified. First, for $\theta_0 < 2$, no morphological transition is expected, since at $\theta_0 \approx 2$ (close to the threshold of sediment transport) t_c is observed to grow markedly (vertical asymptote). In the second place, for

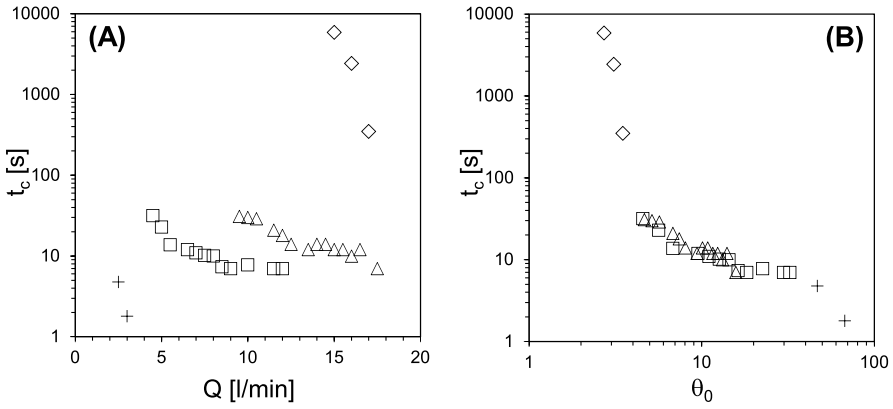

Fig. 5. Critical time, t_c, for the morphological transition: (A) variation of t_c with Q, for different apertures, b_0, and (B) the same data in terms of θ_0. Markers are (see Table 1): $+$ $b_0 = 0.2$ cm, $\square$ $b_0 = 1.0$ cm, $\triangle$ $b_0 = 2.0$ cm and $\lozenge$ $b_0 = 4.0$ cm.

$\theta_0 > 35$, the curve drops abruptly to very small values of t_c: the morphological transition takes place virtually at the beginning of the scour process. In the range $2 \leq \theta_0 \leq 35$ the morphological transition occurs at well defined, finite values of t_c.

For $t > t_c$, see Fig. 4, the erosive work of the jet continued increasing the size of the hole and of the mound, but the sediment transport rate decreases for to two reasons. First, the region where the jet impinges the bed is increasingly far away from the inlet, due to the erosive work. As this distance increases, the jet velocities in this region decrease due to the jet spreading. The sediment transport weakens until reaching the critical distance where the jet is unable to move more grains [15]. In the second place, an increasing amount of grains accumulates on the left side of the mound, due to the jet deviation towards the free surface. Hence, the flow needs more and more time to drag only a few grains above the mound peak, and a close-to-asymptotic stage of erosion is reached. Two erosional regimes were observed to occur during this long-term scour stage, depending on the value of θ_0, as it will be described in the next section.

4.2. The long-term scour regime

Fig. 6 shows two snapshots, taken 1 h apart, for a typical run in the so-called steady recirculation (SR) regime. As can be observed, the peak and the endpoint of the mound stayed virtually immovable (see the vertical dashed lines), and the maximum scour depth has also remained virtually constant. Inside the granular wedge (the triangle whose base is the segment from the peak of the mound to the point of maximum scour depth, approximately), the grains were observed to flow downslope, with each grain moving in contact with its neighbours, closing a steady, clockwise loop. This recirculation pattern has not been reported earlier in studies of erosion caused by two-dimensional wall jets.

Above a critical flow rate, the SR configuration cannot be long sustained and the system undergoes a further transition, to a digging–refilling (DR) regime. During the digging phase, the hole and the triangular wedge grow and the angle of the jet deviation increases following the slope of the right side of the hole. At the end of the digging phase, just before the avalanche, the jet is pointing nearly towards the vertical, see the displacement of the bump at the free surface in Fig. 7(A). The violence of the scour is evidenced by the number of grains kept in suspension, up to a height of about 2/3 of the tailwater depth. When the jet is no longer able to support the triangular wedge, a gravity-driven, sudden avalanche occurs, partially refilling the hole, see Fig. 7(B). After the avalanche, the bottom has almost flattened, see Fig. 7(B), and the jet abruptly deviates towards the main flow direction, recommencing a new digging phase. As in SR configuration, the angle at the right side

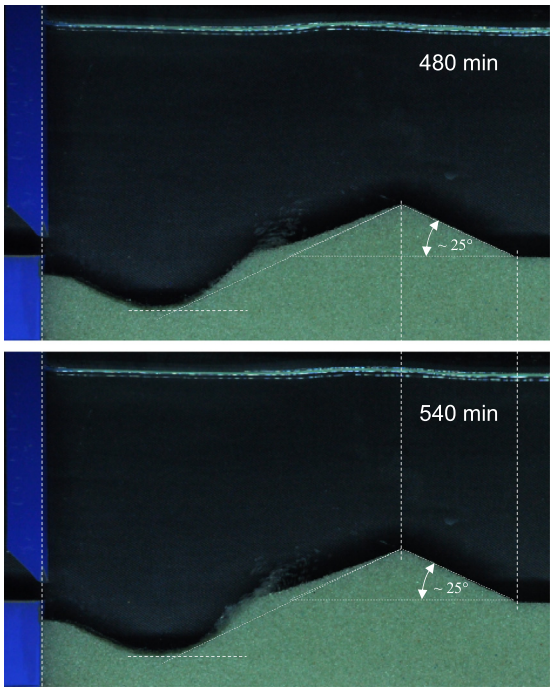

Fig. 6. The steady recirculation (SR) regime, for $b_0 = 1$ cm and $Q = 6.5$ l/min.

of the mound remained about 25° in all cases, which is close to the static angle measured in submerged granular piles [25]. Thus, a configuration in the DR regime displays periodic oscillations in shape and size of both, the hole and the mound. The cycle showed a well defined period, T, measured as $T = T_{di} + T_{fi}$, where T_{di} and T_{fi} are the duration of digging and filling phases, respectively [23]. In all runs avalanches occurred quite abruptly, hence $T_{fi} \ll T_{di}$. Hence, DR cycle in the narrow flume differs substantially from that described earlier, driven by the jet-flipping instability [23,14]. In those cases, the scour hole was observed to grow while the jet was directed toward the bed, whereas the refilling took place when the jet flips towards to the free surface, and the grains were dragged by an inward flow, directed toward the hole. Thus, low refilling rates were observed, due to the weakness of the returning flow, and the cycle was observed to last large timespans, in the order of hours.

The above discussion can be quantitatively summarized by plotting the temporal evolution of the maximum scour depth, Y_0, see Fig. 8. Each curve can be divided into three stages: the short-term phase, where an intense extraction of sediment occurs in a short

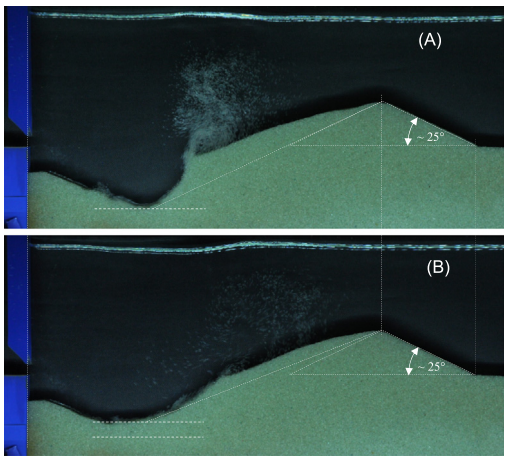

Fig. 7. The digging–refilling (DR) regime, for $b_0 = 1$ cm and $Q = 10$ l/min. Timespan between snapshots (A) and (B) is $T_{fi} \approx 1.7$ s.

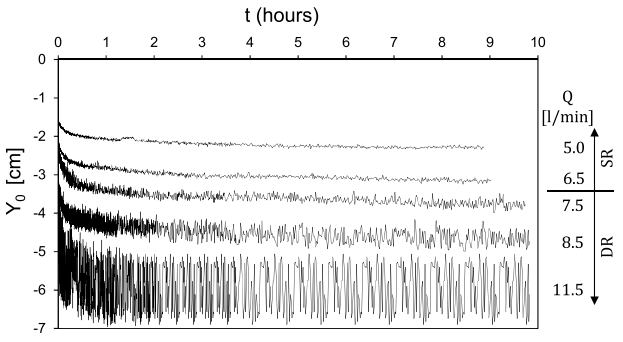

Fig. 8. Temporal evolution of the maximum scour depth, Y_0, for increasing flowrate, Q, and $b_0 = 1$ cm.

time span, followed by the development phase, where the scour process slows down, and, finally, the long-term phase, with Y_0 approaching an asymptotic mean value, Y_∞. Earlier studies of bed scour caused by turbulent two-dimensional jets described such logarithmic dependence [17–19]. But, unlike those results, in the present configuration, the curves display a remarkable change at the critical value $Q^* = 7.5$ l/min. For $Q < Q^*$, the signal presents small oscillations around Y_∞, corresponding to the experimental uncertainties from image processing: the system is in the SR regime. For $Q \geq Q^*$, the oscillations, whose amplitude increases as Q increases, are larger than the experimental uncertainty: the system is in DR regime, and the oscillations correspond to actual variations of the hole depth.

The representative value for Y_∞ was calculated averaging the last 200 points of each series. The amplitude of the oscillation around Y_∞ was estimated through the corresponding standard deviation, σ_∞. Fig. 9(A) presents Y_∞, made dimensionless with b_0, as a function of $Sh_0 = F_0^2$, and Fig. 9(B) displays the same points, but in terms of Y_∞/D_h and θ_0. Data sets of erosion under two-dimensional wall jet [18,24] are also included. From the comparison, it is concluded that the dimensionless numbers used in (B) improves the gathering of the points around a master curve, for a wide range of aspect ratios, $0.5 \leq AR \leq 87$, relative roughness, $0.04 \leq d_s/D_h \leq 0.34$ and the Reynolds number, $3800 \leq Re_0 \leq 75350$. The smallest scour depths (of the order of the grain size) occurred for $\theta_0^c \approx 1,6 \pm 0,3$, near the threshold for sediment motion, where the jet flowed on an almost flat rough bed. For values of $\theta_0 > \theta_0^c$, $Y_\infty/D_h \approx \theta_0^{3/2}$. This scaling shows the effect of increasing the proximity of the side walls: for given values of θ_0 and b_0, scour holes tend to be smaller with decreasing $AR = w/b_0$.

Fig. 10 shows that when the aspect ratio of the hole, Y_∞/X_∞ [18, 21] is plotted against θ_0, most points gather along a kind of master curve. In spite of some scatter, the trend of the points suggests a power-law dependence with exponent $\approx 1/6$. Only a few points deviate from this trend, at $\theta_0 \approx \theta_0^c$, where the experimental uncertainty made it difficult to define X_∞. Since $Y_\infty/X_\infty < 1$, scour in the narrow flume develops slightly elongated holes. This feature was also reported in scour holes from two-dimensional jets [18,24], whose points are also included in the figure. It was observed that the impinging point of the laterally bounded jet was close to (X_∞, Y_∞). Being $\phi = \arctan(Y_\infty/X_\infty)$ the angle of the jet axis with respect to the horizontal, it is concluded that the jet always impacted the bed pointing downward with ϕ from 22° to 39°, approximately.

As it was previously described, see Fig. 8, the transition from SR to DR regimes, at $Q \geq Q^*$, is followed by an increase in σ_∞, beyond the experimental uncertainty. Fig. 11(A) summarizes this finding for all runs (except for $b_0 = 4$ cm, where with the available values of Q it was not possible to attain runs in DR regime). Fig. 11(B) shows that all points also gather along a single, rising curve if σ_∞/D_h is plotted against θ_0. Unlike the previous plots, it was observed that σ_∞/D_h do not follow a power-law function with θ_0. At $\theta_0^* \approx 10$, a sudden change in the trend of the curve is present. This critical value corresponds to the transition from SR to DR regimes. Thus, the proposed dimensionless numbers allow identifying the transition of the scour regimes.

The period, T, for the DR cycle, was measured recording the motion of the point of maximum scour depth, X_∞, with a CCD monochrome camera at 10 fps during 30 cycles. Fig. 12 shows a

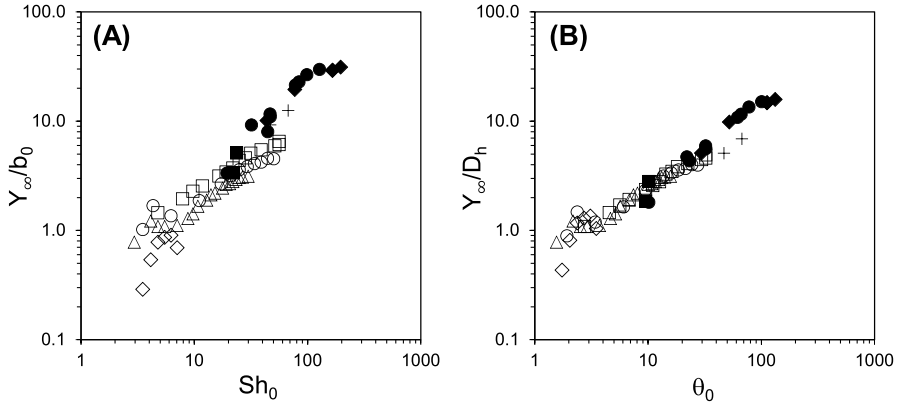

Fig. 9. Dimensionless scour depth as a function of jet strength: (A) Y_∞/b_0 against $Sh_0 = F_0^2$, (B) Y_∞/D_h against θ_0. Markers are (see Table 1): + $b_0 = 0.2$ cm, □ $b_0 = 1.0$ cm, ○ $b_0 = 1.5$ cm, △ $b_0 = 2.0$ cm, ◇ $b_0 = 4.0$ cm., ● Rajaratnam $d_s = 2.4$ mm, ♦ Rajaratnam $d_s = 1.2$ mm and ■ Kurniawan $d_s = 2.0$ mm.

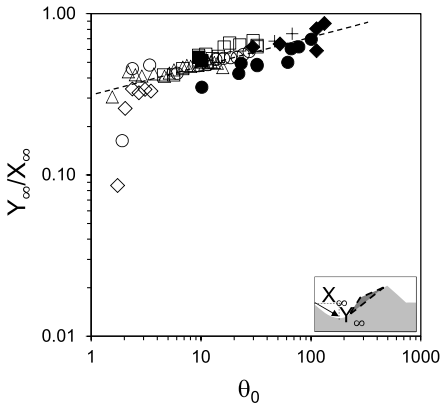

Fig. 10. Scour hole aspect ratio, Y_∞/X_∞, against θ_0. Markers are the same as in Fig. 9.

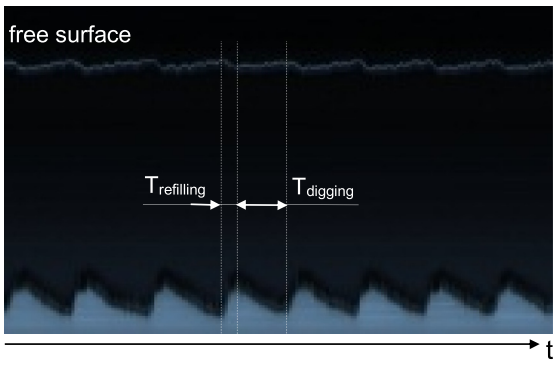

Fig. 12. Typical spatiotemporal diagram for the motion of the point of maximum scour depth in DR regime.

portion of a typical spatiotemporal for the vertical line through this point. The plot shows a sawtooth-like wave: the steepest side (lasting T_{fi}) corresponds to the refilling phase, and the gentle side (lasting $T_{di} \gg T_{fi}$) to the digging phase. The period for the ith cycle was then computed as $T_i = T_{fi} + T_{di}$. The figure also shows the correlation between the location of the maximum scour depth and the level of the free surface just above this point. The free surface level increases due to the progressive deviation of the jet, towards the vertical, during the digging phase. A sudden decrease in the free surface level occurs, following the abrupt change of the jet direction after the avalanche refilled the hole.

Fig. 13(A) displays the period T, calculated as the averaged value over the complete signal, as a function of Q, for each aperture b_0. It is seen that T remains almost constant for a given b_0, and increases with b_0 for a given Q. The increasing dependency of T with b_0 suggest a functional relationship of T with $AR = w/b_0$. Additional measurements were performed, taking advantage of the independence of T with Q, to study this dependency with the widest data set as possible. Several apertures, b_0, were tested at the maximum available value for Q. The value of T was measured after 9 *hs*, following the same protocol previously described. Runs using glass beads of $d_s = 2$ mm were also performed. Fig. 13(B) shows that almost all points gather around a single monotonically decreasing curve. A noteworthy result, deserving future research, is the insensitivity of T with d_s.

4.3. The structure of the mobile granular fraction

The internal structure of the triangular wedge was further study due to the key role played by the grains flow, downhill inside this region. Grey-level maps were computed (from the standard deviation of grey levels at each pixel in the stack) from the last 20 snapshots of each run (covering 1 h of the erosive process). Thus, locations with immobile grains look black, while grey zones correspond to regions with grains in motion. The lighter the grey, the more intense the grains motion is.

Fig. 14(A) displays the map for a run in the SR regime. The granular wedge appears well defined in light grey, bounded from below by a black triangle (whose sides angles are $\approx 25°$) of motionless grains. The thin, lighter bands on the rim of the hole and on the left side of the mound are the grains dragged from the hole, settling above the granular wedge. At the right side of the mound, a very thin light grey band is observed. The dark grey near the maximum scour depth corresponds to the steady stage with Y_∞ constant and small σ_∞. The narrow bump at the free surface corresponds to the virtually steady direction of the jet in this configuration. Fig. 14(B) shows the increase in the size of the triangular wedge for scour in the DR regime. It is also noticeable the increase in the thickness of the grey region close to the maximum scour depth, because of the digging–refilling cycles. The black triangle (immovable grains) below the granular wedge is also well defined, and a very thin light grey band is visible at the right side of the mound. The bump of the free surface is less localized than in SR cases due to the periodic deviation of the jet.

The area occupied by the granular wedge, M, was measured from the grey levels maps. This magnitude is relevant, since it is directly related with the mass of grains $m \simeq \rho_s M w(1-\epsilon)$ in this region, being ϵ the bed porosity. Fig. 15 shows that most of the points gather along a single master curve when M/D_h^2 is plotted against θ_0, following a power law relationship with an exponent

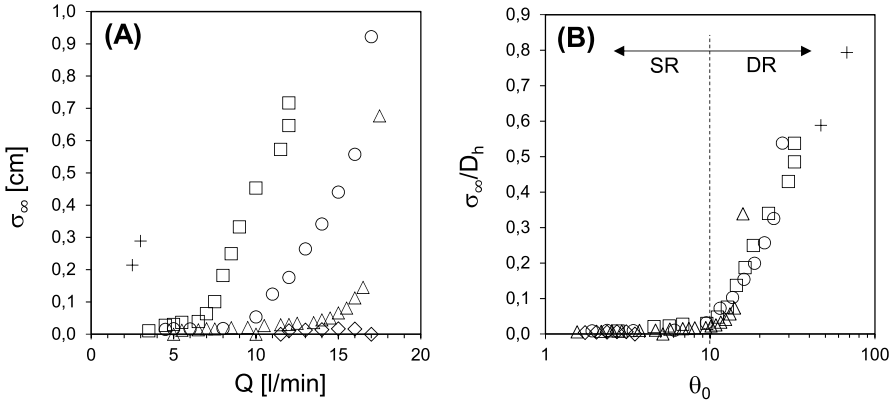

Fig. 11. Standard deviation, σ_∞, of scour depth: (*A*) dependence with Q, parametric in b_0, and (*B*) the same data in terms of dimensionless variables σ_∞/D_h and θ_0. Markers are the same as in Fig. 9.

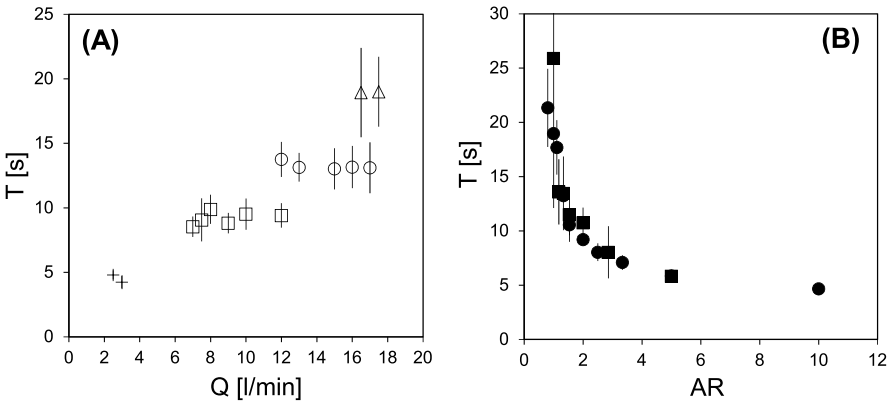

Fig. 13. Period, T, in DR series: (A) as a function of the flow rate, Q, parametric in b_0, markers are as in Fig. 9, and (B) as a function of AR, markers are: ■ $d_s = 2.0$ mm, and ● $d_s = 1.1$ mm. Vertical bars indicate standard deviation.

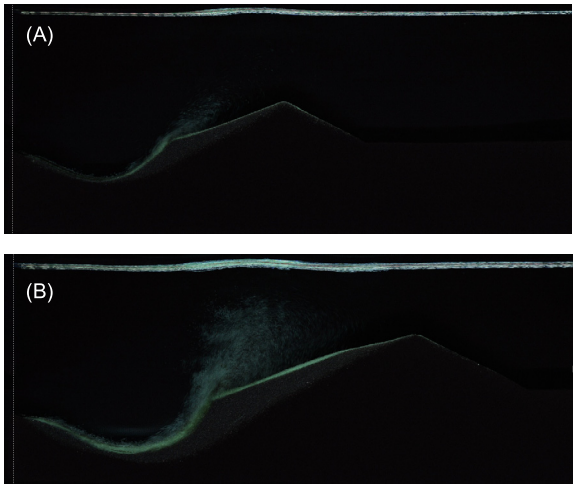

Fig. 14. Grey-levels maps for two runs, $b_0 = 1.5$ cm: (A) SR regime, $Q = 10$ l/min, and (B) DR regime, $Q = 14$ l/min.

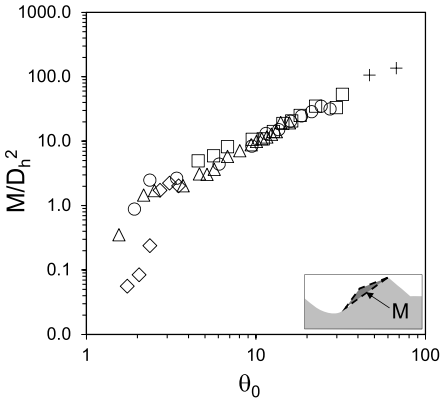

Fig. 15. Dimensionless area of the recirculation wedge, M/D_h^2, against θ_0. Markers are the same as in Fig. 9.

≈ 1. Only a few points fall off this trend, close to $\theta_0 \approx \theta_0^c$, where recirculation regions were small and difficult to identify. Since M was obtained by averaging over several cycles, the curve does not reveal the SR to DR transition at $\theta_0 = \theta_0^*$.

It was observed that the larger M, the larger was the slope of the right side of the hole, see Fig. 14. Hence, the granular wedge is increasingly unstable with increasing values of θ_0, since the component of the weight along the incline could become larger than the hydrodynamical force supporting it. As was discussed above, for $\theta_0 > \theta_0^*$ the granular avalanche cyclically triggers. Thus, the equilibrium condition for a granular wedge impinged by an inclined jet is worth of future research.

5. Conclusions

The effect of lateral confinement due to the very close spacing of the side walls, on the scour of a layer of cohesionless sediment immediately downstream a rectangular sluice gate, has been experimentally studied in a narrow laboratory flume, for jet aspect ratios in the range $0,5 \leq AR = w/b_0 \leq 10$ and several inlet velocities. Time-averaged velocity profiles, measured with PIV for $AR = 1$ in presence of a smooth, no erodible bottom, revealed self-similar velocity distributions, with the structure of a wall jet. Velocity profiles present a noticeable upward-shift when compared to the classical profile for two-dimensional wall jets ($AR \gg 1$). The increase in the thickness of the inner boundary layer indicates a noticeable difference between laterally confined and two-dimensional wall jets. A morphological transition of the downstream mound, from triangular to trapezoidal, took place at the early stage of the erosive process. Such holes with double slopes (resembling an inner–outer crater structure) had not been observed in previous studies of erosion by wall jets issuing from wide rectangular apertures ($AR \gg 1$). This transition was always accompanied by a significant deviation of the jet towards the free surface. Inside the granular wedge (originated by the excess of grains between triangular and trapezoidal profiles) grains move downhill by gravity. This steady recirculation regime (SR) seems to be characteristic of the scour process in the narrow flume. Besides the SR regime, a digging–refilling (DR) cycle was found, where the wedge cyclically destabilizes, triggering an avalanche with well-defined amplitude and period (of about seconds). This cycle is quite different from digging–refilling cycles reported earlier, under wide jets, associated with the jet-flipping instability, which develops in periods of hundreds of hours. The aspect ratio of the jet inlet, AR, plays a relevant role in the definitions of both, the length scale and the Shields number of the erosive process. The new set of dimensionless numbers allowed to gather our experimental points, and those from experiments on scour in wide flumes, in a master curve. Results of this detailed study may be useful to a better understanding of sediment transport processes by highly-confined flows and could help for the validation of new numerical methods.

Funding

The authors gratefully acknowledge the financial support (UBACyT 20020100100853) from Universidad de Buenos Aires, Argentina.

References

[1] Y. Liu, S. Li, Influence of particle size on non-Darcy seepage of water and sediment in fractured rock, SpringerPlus 5 (2016) 2099, http://dx.doi.org/10.1186/s40064-016-3778-9.

[2] N. Patankar, D. Joseph, J. Wang, R. Barree, M. Conway, M. Asadi, Power law correlations for sediment transport in pressure driven channel flows, Int. J. Multiph. Flow. 28 (2002) 1269–1292, http://dx.doi.org/10.1016/S0301-9322(02)00030-7.

[3] V. Matouek, Research developments in pipeline transport of settling slurries, Powder Technol. 156 (2005) 43–51.

[4] M. McClure, Bed load proppant transport during slickwater hydraulic fracturing: Insights from comparisons between published laboratory data and correlations for sediment and pipeline slurry transport, J. Petrol. Sci. Eng. 161 (2018) 599–610, http://dx.doi.org/10.1016/j.petrol.2017.11.043.

[5] I. Tomac, D.M. Tartakovsky, Experimental evaluation of turbulent flow and proppant transport in a narrow fracture, in: PROCEEDINGS, 43rd Workshop on Geothermal Reservoir Engineering, Stanford University, SGP-TR-213, 2018, pp. 1-9.

[6] M. Biot, W. Medlin, Theory of sand transport in thin fluids, in: 60th Annual Technical Conference and Exhibition of the Society of Petroleum Engineers (SPE), Vol. 14468, 1985, pp. 1-24.

[7] A. Canestrelli, W. Nardin, D. Edmonds, S. Fagherazzi, R. Slingerland, Importance of frictional effects and jet instability on the morphodynamics of river mouth bars and levees, J. Geophys. Res. Oceans 119 (2014) 509–522, http://dx.doi.org/10.1002/2013JC009312.

[8] S. Pagliara, I. Carnacina, Temporal scour evolution at bridge piers: effect of wood debris roughness and porosity, J. Hydraul. Res. 48 (1) (2010) 3–13, http://dx.doi.org/10.1080/00221680903568592.

[9] A. Khosronejad, C.D. Rennie, Three-dimensional numerical modeling of unconfined and confined wall-jet flow with two different turbulence models, Can. J. Civil Eng. 37 (2010) 576–587, http://dx.doi.org/10.1139/L09-172.

[10] J. Guo, P. Julien, Shear stress in smooth rectangular open-channel flows, J. Hydraul. Eng. 131 (1) (2005) 30–37.

[11] M. Alnahhal, A. Cavo, A. Romeos, K. Perrakis, Th. Panidis, Experimental investigation of the effect of endplates and sidewalls on the near field development of a smooth contraction rectangular jet, Eur. J. Mech. B Fluids 30 (2011) 451–465.

[12] A. Abdel-Rahman, A review of effects of initial and boundary conditions on turbulent jets, WSEAS Trans. Fluid Mech. 4 (5) (2010) 257–275.

[13] M. Shestakov, V. Dulin, M. Tokarev, D. Sikovsky, D. Markovich, PIV study of large-scale flow organisation in slot jets, Int. J. Heat Fluid Flow 51 (2015) 335–352.

[14] A. Bey, M. Faruque, R. Balachandar, Effects of varying submergence and channel width on local scour by plane turbulent wall jets, J. Hydraul. Res. 46 (6) (2008) 764–776, http://dx.doi.org/10.1080/00221686.2008.9521921.

[15] S. Badr, G. Gauthier, P. Gondret, Erosion threshold of a liquid immersed granular bed by an impinging plane liquid jet, Phys. Fluids 26 (2014) 023302, http://dx.doi.org/10.1063/1.4863989.

[16] B.W. Melville, Scour at various hydraulic structures: sluice gates, submerged bridges, low weirs, in: Hubert Chanson and Luke Toombes, Hydraulic structures and society - Engineering challenges and extremes. 5th IAHR International Symposium on Hydraulic Structures, ISBN: 9781742721156, Brisbane, Australia, 2014, http://dx.doi.org/10.14264/uql.2014.10.

[17] M. Aamir, Z. Ahmad, Review of literature on local scour under plane turbulent wall jets, Phys. Fluids 28 (2016) 105102, http://dx.doi.org/10.1063/1.4964659.

[18] N. Rajaratnam, Erosion by plane turbulent jets, J. Hydraul. Res. 19 (4) (1981) 339–358, http://dx.doi.org/10.1080/00221688109499508.

[19] R. Balachandar, H. Reddy, Scour caused by wall jets, in: Andrew J. Manning (Ed.), Earth and Planetary Sciences - Sediment Transport Processes and their Modelling Applications, ISBN: 978-953-51-1039-2, 2013, pp. 177–210, Chapter 8.

[20] P. Sarathi, M. Faruque, R. Balachandar, Influence of tailwater depth, sediment size and densimetric Froude number on scour by submerged square wall jets, J. Hydraul. Res. 46 (2) (2008) 158–175, http://dx.doi.org/10.1080/00221686.2008.9521853.

[21] A.J. Hogg, H.E. Huppert, W.B. Dade, Erosion by planar turbulent wall jets, J. Fluid Mech. 338 (1997) 317–340, http://dx.doi.org/10.1017/S0022112097005077.

[22] M.A.A. Faruque, P. Sarathi, R. Balachandar, Clear water local scour by submerged three-dimensional wall jets: Effect of tailwater depth, J. Hydraul. Eng. 132 (6) (2006) 575–580.

[23] C. Xie, S.Y. Lim, Effect of jet-flipping on scour development downstream of a sluice gate, in: 6th. International Conference on Scour and Erosion (ICSE 6), Paris, France, 2012.

[24] A. Kurniawan, M. Altinakar, W. Graf, Scour depth and flow pattern of eroding plane jets, Int. J. Sediment Res. 19 (1) (2004) 15–27.

[25] S. Courrech du Pont, P. Gondret, B. Perrin, M. Rabaud, Wall effects on granular heap stability, Europhys. Lett. 61 (4) (2003) 492–498, http://dx.doi.org/10.1209/epl/i2003-00156-5.

[26] T. Loiseleux, P. Gondret, M. Rabaud, D. Doppler, Onset of erosion and avalanche for an inclined granular bed sheared by a continuous laminar flow, Phys. Fluids 17 (2005) 103304, http://dx.doi.org/10.1063/1.2109747.

[27] J.G. Eriksson, R.I. Karlsson, J. Persson, An experimental study of a two-dimensional plane turbulent wall jet, Exp. Fluids 25 (1998) 50–60.

[28] N. Rostamy, D.J. Bergstrom, D. Sumner, J.D. Bugg, Incomplete Similarity of the Plane Turbulent Wall Jet, Proceedings of 7th International Symposium on Turbulence and Shear Flow Phenomena (TSFP7), Vol. 2, Ottawa, Canada, 2011.

[29] S.A. Ead, N. Rajaratnam, Plane turbulent wall jets in shallow tailwater, J. Eng. Mech. 128 (2) (2002) 143–155.

[30] A. Verhoff, The two dimensional turbulent wall jet with and without an external stream, Rep. 626, Princeton University, New Jersey, USA, 1963.

[31] S. Bennett, C. Alonso, Kinematics of flow within headcut scour holes on hillslopes, Water Resour. Res. 41 (2005) W09418, http://dx.doi.org/10.1029/2004WR003752.

[32] N. Rostamy, D.J. Bergstrom, D. Sumner, J.D. Bugg, An experimental study of a turbulent wall jet on smooth and transitionally rough surfaces, J. Fluids Eng. 133 (11) (2011) 111207, http://dx.doi.org/10.1115/1.4005218.

[33] Z. Tang, D.J. Bergstrom, J.D. Bugg, A plane turbulent wall jet on a fully rough surface, Int. J. Heat Fluid Flow 66 (2017) 258–264.

[34] R.C. Deo, J. Mi, G.J. Nathan, The influence of nozzle aspect ratio on plane jets, Exp. Therm Fluid Sci. 31 (2007) 825–838.

[35] C. LaMarche, J. Curtis, Cratering of a particle bed by a subsonic turbulent jet: Effect of particle shape, size and density, Chem. Eng. Sci. 138 (2015) 432–445, http://dx.doi.org/10.1016/j.ces.2015.08.030.

[36] O.O. Aderibigbe, N. Rajaratnam, Erosion of loose beds by submerged circular impinging vertical turbulent jets, J. Hydraul. Res. 34 (1) (1996) 19–33, http://dx.doi.org/10.1080/00221689609498762.